SHEAR WAVE GENERATION BY DECOUPLED AND PARTIALLY COUPLED EXPLOSIONS

Jeffry L. Stevens, Heming Xu, and G. Eli Baker

Science Applications International Corporation

Sponsored by Air Force Research Laboratory

Contract No. FA8718-06-C-0007
Proposal No. BAA06-46

ABSTRACT

The objective of this project is to investigate the sources of shear wave generation by decoupled and partially coupled explosions, and the differences in shear wave generation between tamped and decoupled explosions. A perfectly spherical explosion at the center of a perfectly spherical cavity large enough to fully decouple the explosion would generate no shear waves, so all shear waves from decoupled explosions are due to asymmetries in and near the cavity, and to scattering and conversions. We quantify the effect of different sources of asymmetry through numerical modeling, and take advantage of unique features of different data sets to eliminate particular mechanisms and so constrain the possible sources of observed shear waves.

We present numerical calculations, and analytic solutions for different pressure functions, of the problem of shear wave generation by an explosion offset from the center of a spherical cavity, which causes the shock wave to vary in amplitude and arrival time around the cavity surface. The offset explosion has a dipole component and can generate significant shear waves with a modest offset from the center. The numerical calculations produce cavity reverberations that are strongest along the axis of the source offset. We develop a physically reasonable pressure function that models the pressure reverberations and show that it leads to longer duration waveforms with more low frequency content, again with a dominant dipole contribution.

We have shown previously that the radiation pattern of the near field, initial, shear-wave arrivals from the decoupled explosion Sterling could be reproduced by modeling that included the flat floor (due to melted and recrystallized salt) of the cavity. The observations also have substantial coda, which are not reproduced by the calculations. Similarity of coda waveforms with distance indicates their source is at or very near the cavity. Longer time modeling of the air shock evolution appears to produce a more realistic source function and provide a better match to the coda. We also assess the likelihood that fractures created by the tamped explosion that formed the cavity, Salmon, were re-opened by Sterling. Modeling of hydrofracture propagation driven by the Sterling explosion, by coupling stress wave dynamics in rock with fluid mechanics in the fractures, shows that the cavity pressure is insufficient to overcome the overburden to propagate fractures into rock, except for the area immediately below the explosion on the cavity floor.

We complete analysis and modeling of local records of a 27 Kt tamped and four smaller (0.01 to 0.35 Kt) water filled cavity explosions. We identify two distinct S-phases, neither of which has the 9 Hz bubble pulse peak that the decoupled explosions' coda and P spectra have, which is inconsistent with generation of the initial shear waves by P-wave scattering. Addition of a compensated linear vector dipole (CLVD) source of comparable moment to a spherical explosion source is necessary to reproduce the observed S-waves. Nonlinear source calculations indicate that neither an offset in the source or fracturing is a likely source of the shear waves.

The Israeli Oron decoupling experiment of 2006 consisted of one tamped and two partially decoupled explosions. The latter were strongly overdriven and have similar waveforms from 1 to 30 Hz, but have distinct differences at higher frequencies. The spectra of each event is very distinct. We use group velocities and particle motion to isolate P and S wave energy in local records, and find that for each event, the P and S spectra are similar, with one exception, the tamped explosion has a smaller S/P ratio at 30 to 50 Hz. This is consistent with S being primarily scattered from P, as is expected for these very shallow events in a low velocity medium. That conclusion is supported by the excellent fit to both P and S waves by point spherical explosion synthetics.

OBJECTIVES

The objective of this project is to investigate the sources of shear wave generation by decoupled and partially coupled explosions, and the differences in shear wave generation between tamped and decoupled explosions. This is being accomplished through a program of data analysis and numerical modeling of decoupled and partially coupled explosions.

RESEARCH ACCOMPLISHED

Introduction

This project investigates shear waves from decoupled and partially coupled explosions, focusing on source mechanisms for shear waves, constrained by observations and numerical simulations. Although a nuclear explosion detonated at the center of a perfect spherical cavity large enough to decouple the explosion would generate no shear waves (other than conversions due to the earth's surface and scattering), in fact no cavity has perfect spherical symmetry, nor is the explosion exactly at the center, and shear waves have been observed from all decoupled explosions, even quite close to the source.

In this paper, we report on the completion of the analysis of three specific problems, previously discussed in Stevens et al (2007), and on preliminary analysis and modeling of a new data set. We present analytic and numerical solutions to the problem of shear waves generated by an explosion offset from the center of a spherical cavity. We complete the analysis and modeling of the Sterling explosion data, focusing on understanding the S-coda waveforms and spectra. We also complete the analysis and modeling of shear waves from nuclear explosions in water-filled cavities. Finally, we analyze and model P and S spectra from Israeli tamped and partially decoupled explosions.

Shear Waves from a Non-Isotropic Explosion Source

In Stevens et al. (2007), we presented a general solution to the problem of shear waves generated by an explosion offset from the center of a spherical cavity. The offset causes a dipole component to the source which generates S waves and causes angular variation in P wave amplitude and shape. By conservation of momentum, the S waves must vanish at zero frequency but they may be a sizeable fraction of the P waves at frequencies of interest. We refine the model of the amplitude function, in particular its dependence on incidence angle, decay with time, and the effect of reverberations, the latter motivated by results of nonlinear axisymmetric calculation of an offset explosion in a spherical cavity.

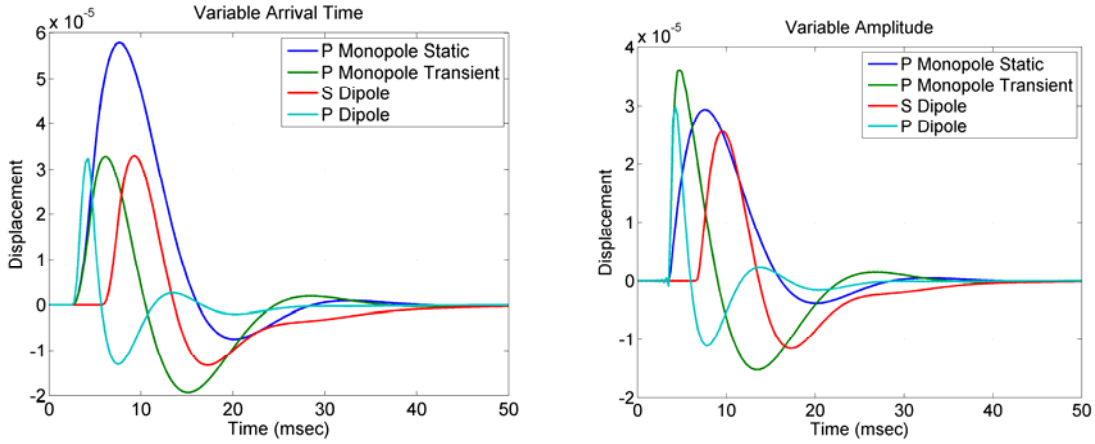

Figure 1. Waveforms of the monopole and two dipole terms for the angle dependent arrival time with constant amplitude (left) and angle dependent amplitude variation (right), both for a point explosion source in a 17 meter radius cavity.

We solve the general problem of the seismic wave field caused by a set of tractions applied to the inside of a spherical cavity. The solution includes terms that represent the response of the medium to the applied stress from the explosion and motion due to the response of the cavity wall. Both the applied pressure and the generated seismic wavefield can be expanded in vector spherical harmonics. The problem simplifies since the applied pressure is normal to the cavity wall. For the simple case where pressure has the same functional form at all points on the cavity

wall, differing only by start time, and has an exponential decay with time, the dipole term produces shear waves that are a significant percent of the P-wave size (Figure 1, left). Results are similar for the case where pressure is higher on the offset side, balanced by longer duration, lower amplitude pressure on the other side (Figure 1, right).

A nonlinear, axisymmetric, Eulerian calculation that simulates the explosion within the cavity and the air-rock interaction produces similar results, but with the addition of complex and persistent cavity reverberations. The calculation is for a 0.38 kiloton explosion in a 17 meter radius air-filled cavity, offset by 5 meters from the cavity center. The yield and cavity size correspond to the Sterling explosion, although we use a strong rock model to prevent the plastic yielding that occurs with salt. The calculation did not include gravity. Figure 2 shows the pressure field at 2.5 msecs, the pressure time histories at different points in the cavity, and P and S velocity waveforms.

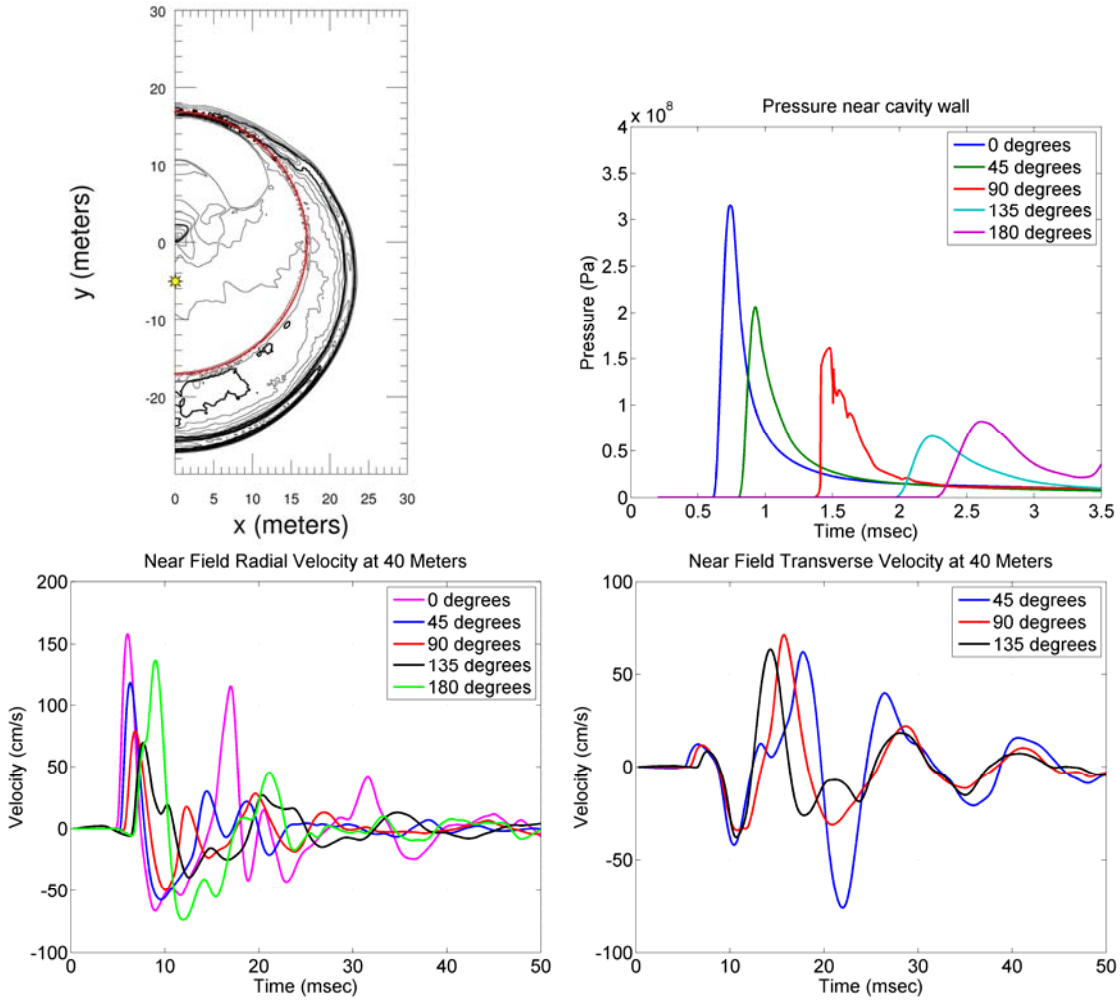

Figure 2. Pressure contours at 2.5 msec (upper left). Red line on the contour plot shows the cavity wall; the yellow mark shows the explosion location. The first 3.5 msec of the pressure time histories at 5 points inside the cavity next to the wall (upper right). Zero degrees is in the direction of the explosion offset toward the bottom of the grid. Radial (bottom left) and vertical (bottom right) velocity waveforms low pass filtered at 200 Hz at a distance of 40 meters from the cavity center.

These results motivate a model of pressure for the analytic solution that more accurately represents the reverberations within the cavity. Specifically, because the pressure pulses are stronger at the ends of the cavity and decline in amplitude with each reverberation, we model the pressure field as a series of transient pressure pulses on each half of the cavity with maximum amplitude at zero and π, varying as cosθ. For a single pressure pulse on each side, the results are similar to the earlier examples. With multiple reverberations, however, the waveforms are longer

and have more low frequency content. Figure 3 shows an example with 10 reverberations, with the pressure decaying exponentially with time.

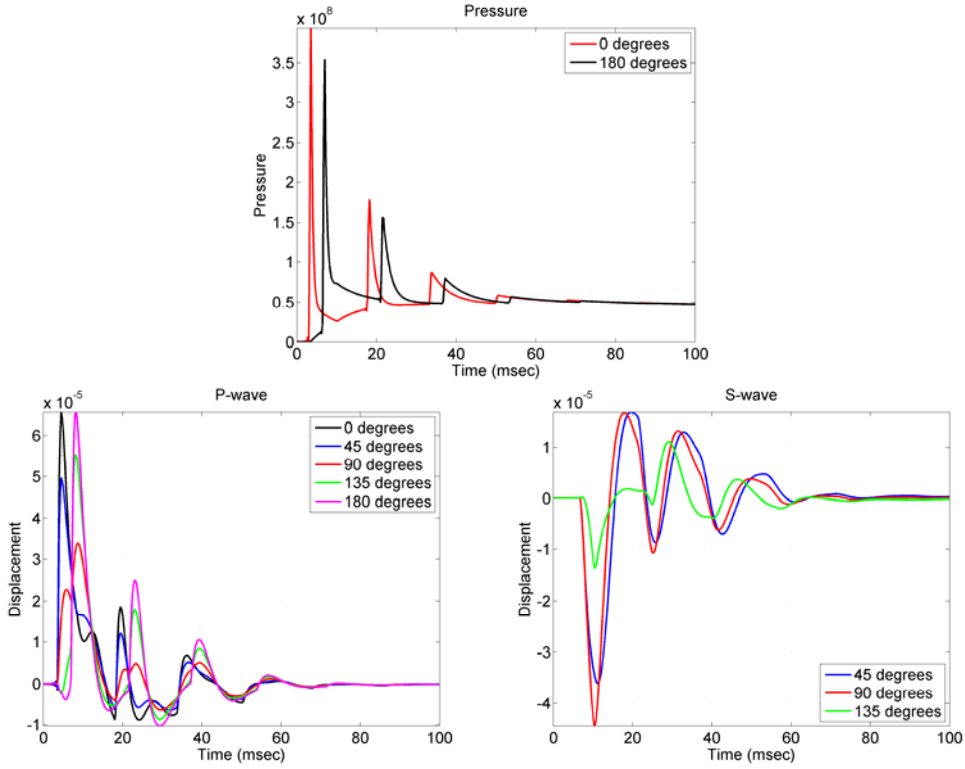

Figure 3. Cavity pressure at 0 (the offset direction) and 180 degrees (top) and far field P and S waves generated by the pressure function.

Sterling Calculations

Stevens et al. (2007) presented simulations of the Sterling explosion, reporting that near field waveforms, including the radiation pattern of the initial arrivals of near field shear waves, can be explained by the cavity shape and the asymmetry caused by varying impact of the explosion shock across different parts of the cavity. Those calculations were based on an initial state, determined using the Eulerian nonlinear code used in the offset source calculations. The calculation was run long enough to get the shock wave well into the surrounding material, and then the results of that calculation defined the initial conditions for a nonlinear Lagrangian finite-difference code that propagated the deformation out beyond the elastic radius. During the overlay the interior of the cavity is rezoned into a single zone with a constant pressure. Stevens et al. (2007) also report on hydrofracture calculations, which indicate that cracking is not likely the source of the observed shear waves. In particular, pressure within the Sterling cavity is not sufficient to open a single preexisting conical crack connecting to the outer bottom edge of the cavity, such as that proposed in the kinematic model of Langston (1983). In the case where cracks are allowed to form anywhere in the medium, the overburden greatly limits the extent of cracking, preventing generation of significant shear wave energy.

Here we address one further aspect of the problem, the reverberations within the coda. Stevens et al (2007) reported that stacks of coda from at, above, and below shot level records showed that the coda are similar at similar incidence, which indicated that the S-wave coda source is located at or very near the cavity. The coda shear waves also have a radiation pattern with incidence, different from that of the initial S-wave, suggesting a different mechanism from that of the initial S.

Figure 4 shows the near field P-wave observations, seismograms and spectra, made above, at, and below shot point, scaled to the most distant location by using Qp=200, and corrected for geometrical spreading. The time series and 30 Hz corner frequency of the observations are well matched by the nonlinear source calculation. The reverberations of the observed S-waves however, are not reproduced by the numerical model (Figure 5). Further, several studies have found that S source spectra are similar to those of P, but with the corner frequencies reduced by the S-to-P velocity

ratio (e.g., Fisk, 2007). For Sterling, the observed S spectra appear to have a much higher frequency corner. The apparent higher corner may be due to a broad resonance peak at 55 Hz. The results of the previous section bear on this result. The nonlinear source calculations took as initial conditions the stress and velocity at all grid points at a single instant, with the exception of the cavity itself, which was then modeled as a simple cavity with constant pressure. This proved very effective for modeling the initial P and S waves, but excluded cavity reverberations. The models presented in the previous section however, explain the observed long duration near field waveforms from Sterling as caused by vertically oriented cavity reverberations.

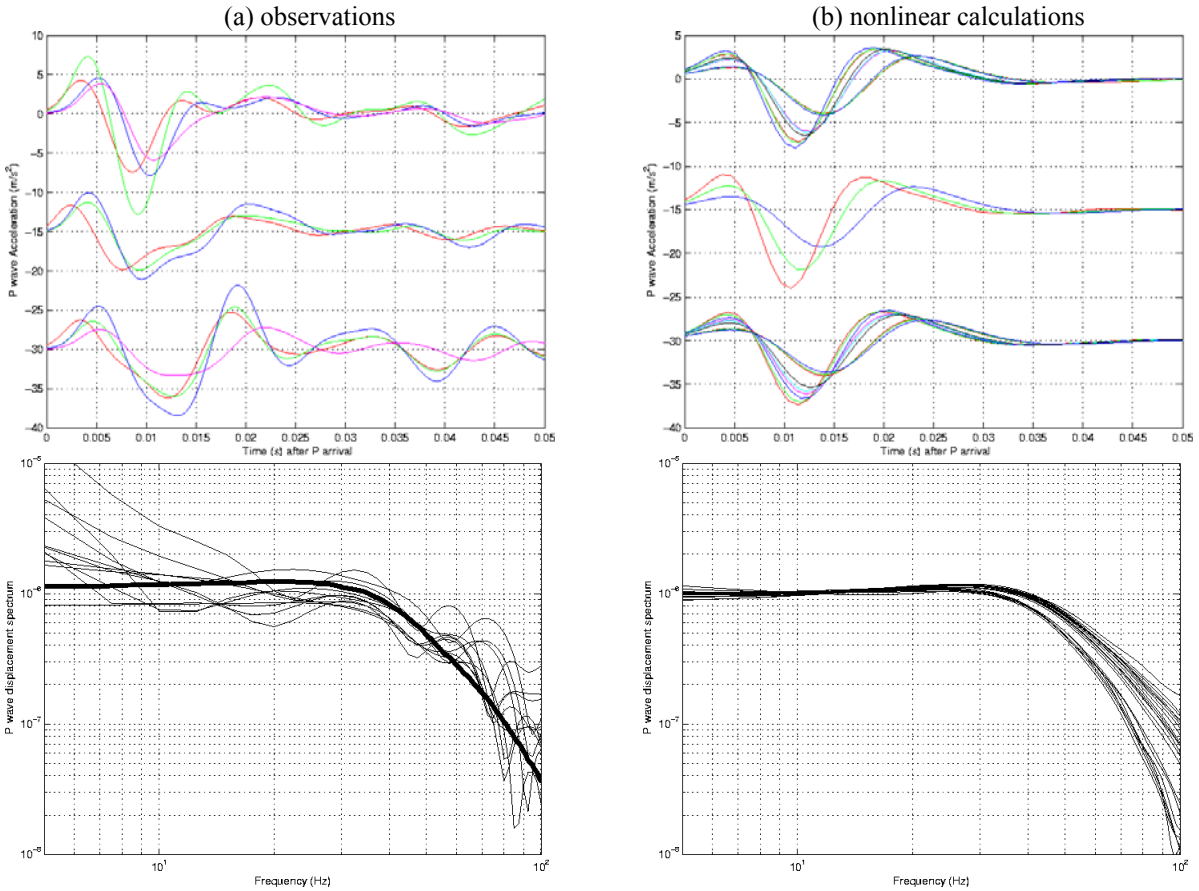

Figure 4. Radial P waveforms aligned at their predicted arrival time and filtered from 3–100 Hz (top) and their spectra (bottom) from the observations (left) and nonlinear calculations (right). The top, middle, and bottom sets of seismograms correspond to receivers above, at, and below the shot level. In the observed spectra (bottom left), the thick line indicates the prediction for a spherically symmetrical case.

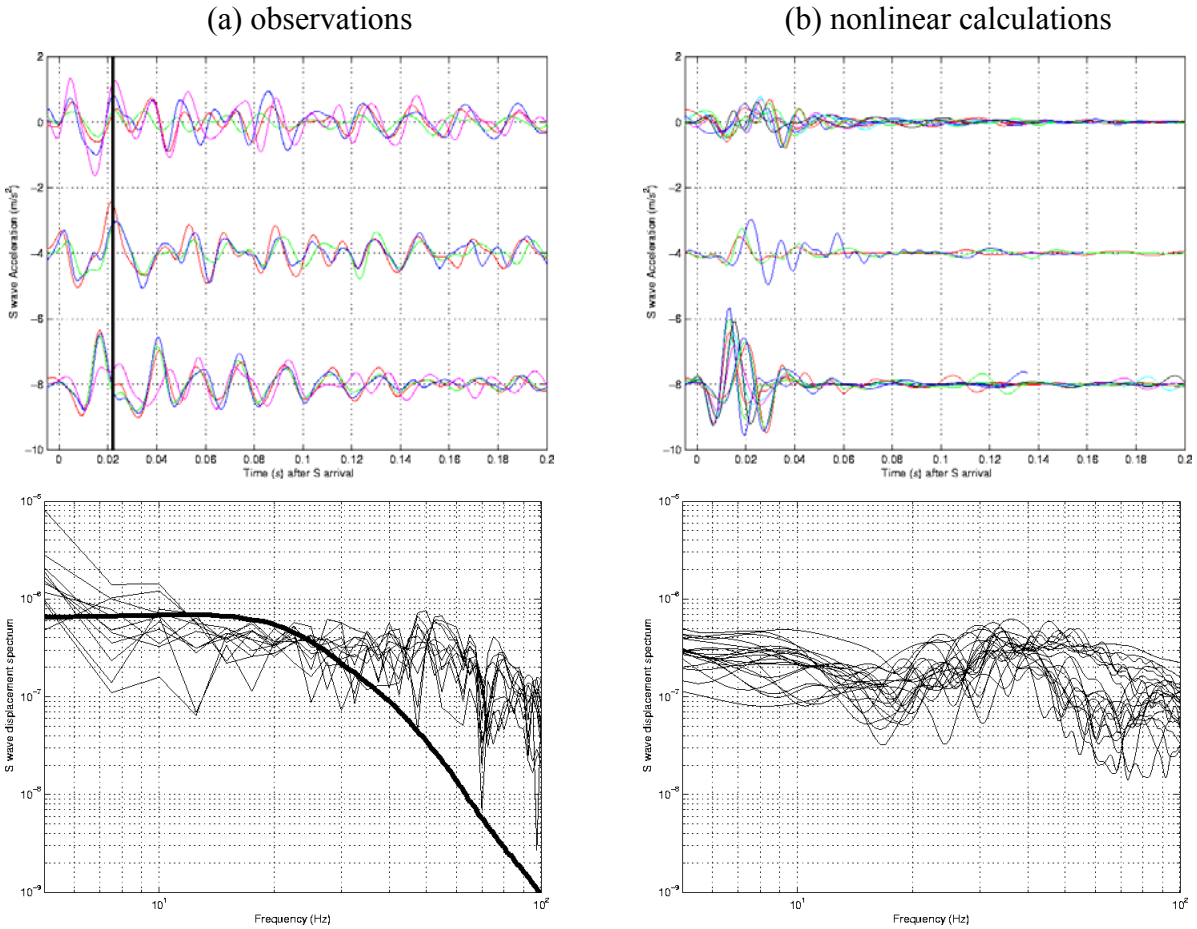

Figure 5. Similar to Figure 4, but for tangential S waveforms. The solid line in the lower left figure shows the predicted spectrum from scaling the P spectrum by the S/P velocity ratio, which is clearly inconsistent with the data. The data can be explained by a vertical dipole source caused by cavity reverberations.

Explosions in Water-Filled Cavities

In Stevens et al. (2007), we presented two independent sets of observations from a unique series of explosions, a tamped 27 Kt explosion at 597 m depth in salt at Azgir, followed by four very small explosions (yields 0.35, 0.10, 0.01, and 0.08 kt) in the water-filled, 32.5 m radius, cavity of the original explosion. These are effectively decoupled, in that the small explosions do not cause significant nonlinear deformation of the cavity, but provide large signals as the pressure is much greater in water than it would be in an air-filled cavity. We showed that the P, but not the S spectra of the decoupled explosions each have a 9 Hz bubble pulse resonance peak, indicating that the S waves were not scattered from P. The explosion depth precludes generation of 9 Hz Rg, so scattered Rg also cannot be the source of S. We also showed that the S travel time curve is consistent with direct generation of S at the source or near instantaneous scattering at the source.

Through further modeling and analysis of travel times and particle motion, we identify two distinct S phases (Figure 6, left). Particle motion of the second S phase is retrograde, consistent with identification as a higher mode surface wave. Equivalently, it is also consistent with shear waves trapped in the low velocity surface layer (the velocity model is provided in Stevens et al, 2007). The particle motion of the initial S wave is more complex, but for most records the motion transitions from linear in the P wave window to more circular in the S window. The travel time of the initial S wave is consistent with the direct arrival and the second is consistent with propagation along the surface. The S is not generated by a point spherical explosion, but requires an S wave source. Phase identification is consistent between events and over the range of distances observed (1 to 9 km).

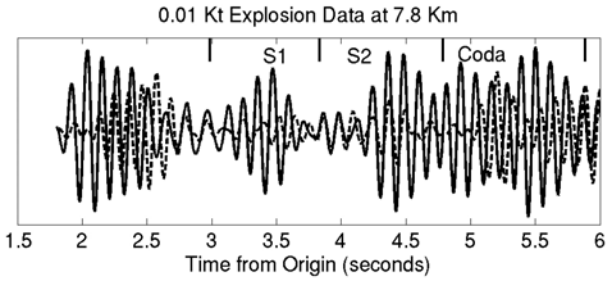

Figure 6. Overlain vertical (solid) and Hilbert transformed radial (dashed) velocity records of the 0.01 Kt explosion at 7.8 km, filtered from 5 to 10 Hz (above). The first and second S arrivals (labeled S1 and S2) and the coda are delimited by vertical bars along the upper plot boundary.

Neither of the shear waves have the bubble pulse peak, but the coda shares the bubble pulse peak with the P wave, demonstrating that a phase scattered at least partly from P will share that spectral feature, further indicating that neither S-wave is scattered from P (Figure 7).

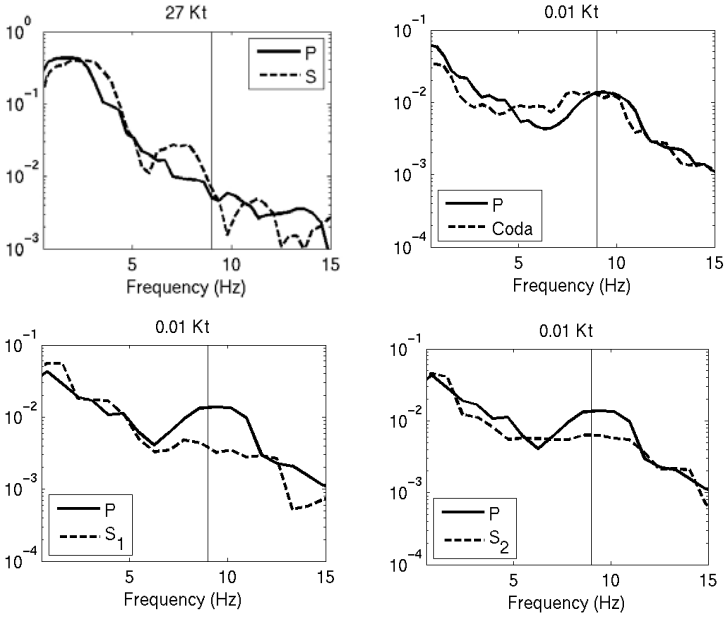

Figure 7. Neither the P or S spectra of the tamped explosion (upper left) have a 9 Hz bubble pulse peak. The P (solid) and coda (dashed) spectra of the 0.01 Kt explosion both have the resonance peak (upper right). Neither the initial S (bottom left) or second S phase (bottom right) have the spectral peak. The results for other decoupled events are consistent.

We estimate the relative size and depth of a CLVD component that is required to match the observations. We match the average of the vertical and radial component amplitudes, and for S, match the sum of the first and second S phase amplitudes. To first order, a CLVD with the same moment as the explosion provides a good match to the observed S-to-P ratio. There is some variability between even the decoupled explosion S-to-P ratios, so it is difficult to draw conclusions regarding second order differences between the decoupled and tamped explosions. Nonetheless, some of the details are interesting. When filtered from 5 to 10 Hz, the CLVD component required to match the observed decoupled explosion S-to-P ratios is significantly smaller than that of the tamped explosion, 41% of the total moment vs. 65%. When filtered from 4 to 8 Hz however, so the bubble pulse peak is excluded, the tamped explosion's CLVD moment relative to the spherical explosion moment is only slightly larger than the decoupled explosions'. Specifically, the CLVD then is, on average, 53% of the total moment of the decoupled explosions, vs 61% for the tamped. There is another difference between the decoupled and tamped events' S-waveforms that may reduce the difference further and shed light on their origins.

The initial S-wave of the tamped explosion is later than that of the decoupled explosions. This would occur if the tamped explosion's S-wave were generated at a shallower depth, as it would then excite slower modes. Figure 8 shows the sum of synthetics for a 597 m depth spherical explosion plus a CLVD of the same amplitude. The upper trace shows the case where the CLVD is at the same depth. The second trace shows the case where the CLVD is at half the depth. The S-wave energy is more strongly concentrated later in the seismogram in the second case. The earlier S arrival of the deeper CLVD source matches the earlier S of the 0.35 Kt event (third trace). All the

decoupled explosions have earlier S. The later arriving S due to greater excitation of higher modes by the shallower CLVD is consistent with the tamped explosion record (bottom).

Besides the effect on timing, a shallower source of the same moment yields larger amplitudes than a deeper source. This is due to greater excitation of the shallow modes and to the effect of depth on the cavity size, the latter of which isn't even reflected in the synthetics shown. This means that the moment of a shallow CLVD source necessary to match the observed S-to-P ratio of the tamped explosion is reduced. Resolution of the predicted amplitudes is limited by uncertainty in the details of the source structure and in the exact depth distribution of the tamped source. To first order however, we conclude that both the decoupled and tamped explosion records require an S-wave source of comparable moment to produce the observed S waves. The significant difference is that for the decoupled explosions, the source is at the spherical explosion depth, and for the tamped explosion, an S-wave source at half the depth provides a better match to the data.

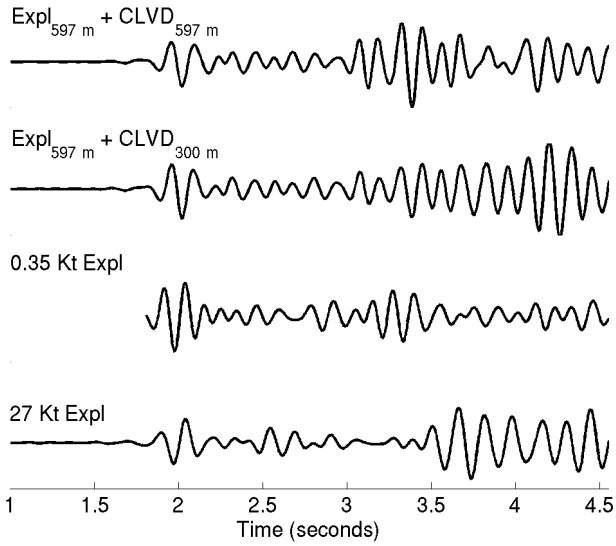

Figure 8. Synthetic vertical seismograms at 7.8 km, filtered from 4 to 8 Hz for an explosion plus a CLVD source of the same moment at the same depth (top), and an explosion plus CLVD source of the same moment but at half the depth (second trace). The deeper CLVD source matches the earlier S of the 0.35 Kt event (third trace), while the shallower CLVD is consistent with the later S energy in the tamped explosion record (bottom).

We performed several nonlinear source calculations to assess the effect of source asymmetries and fracturing, including calculations with the explosion at the top, center, and base of the cavity. Figure 9 shows the nonlinearly deformed areas in each of those cases. The hard anhydrite cap flattens the upper surface, and when the explosive is detonated at the base of the cavity, the deformation extends much further downward. Surprisingly however, the records of each are very similar to that of a spherical point explosion. Additional asymmetry of some sort is required to match the data, indicating that we are imposing more symmetry on the solution that actually exists.

We also performed fracture calculations. The first assessed the ability of the explosion to drive open pre-existing cracks connected to the cavity, where all the material about the cavity is fractured. In that case, with overburden pressure of about 130 bars and peak cavity pressure for the 0.35 Kt explosion at 269 bars, the dynamic region extends only 3 m into the salt and has no obvious preferred direction. The effect on the seismograms is not significant. We also performed a calculation with a horizontal crack radiating out from the cavity. As with the hydrofracture calculation, the peak cavity pressure of 269 bars overcomes the overburden of 130 bars, and so opens the crack outward 50m into the salt in the initial 300 ms and then closes to within 1 m of the cavity due to depletion of the cavity pressure. Again, however, the waveforms outside of the near field are similar to those of a spherical explosion source.

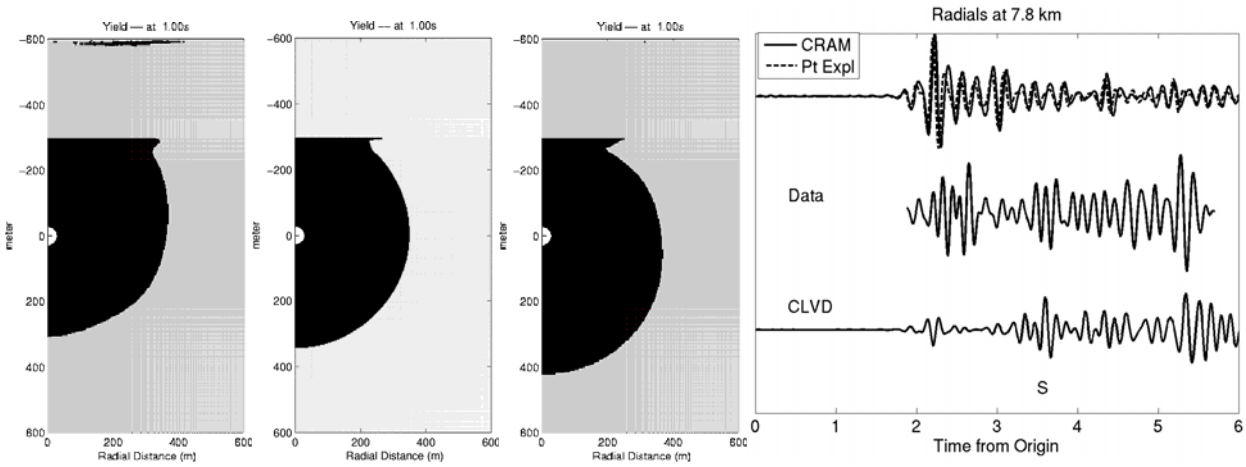

Figure 9. Nonlinear yield region around the cavity for the 0.35 Kt explosion placed at the top, center, and bottom (left to right respectively) of the cavity. The rightmost plot shows radial seismograms at 7.8 km. The record from the calculation with the explosion at the center (upper trace, solid) is overlain with that from a spherical point explosion source (upper trace, dashed), and is compared with data (middle trace) and CLVD synthetics (bottom trace).

Israeli Decoupling Experiment

We have performed preliminary analysis and modeling of data from the Israeli decoupling experiment (Gitterman et al., 2007), which included three explosions, each of 1,240 kg of ANFO, one tamped at 30 m depth, one at the base of a 26.5 m deep, 4 m^3 cavity, and one at the base of a 60 m deep, 14 m^3 cavity. All were recorded on a common set of local to regional stations. We have identified the local P and S wave phases, investigated whether there are differences between those phases from the different events, and modeled the observations.

Although spectral differences exist between events, first order differences do not appear to exist between the P and S phases for a single event. Figure 10 shows the vertical P compared with the tangential S spectra for each event. For the most part, the S spectra is similar to the P, with the exception that there may be less S wave energy from 30 to 50 Hz from the tamped explosion.

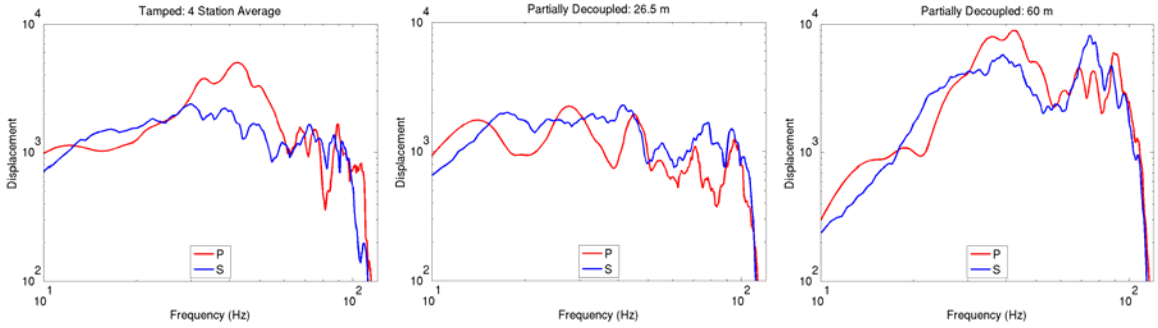

Figure 10. Vertical P (red) and tangential S (blue) spectra from the tamped (left), and two partially decoupled explosions (center and right, 26.5 and 60 m depth respectively).

Similar S to P spectra is consistent with conversion from P being the dominant source of S-waves. The velocity is very low at the source (Gitterman et al., 2007), so we expect pS to be trapped, plus the very shallow source depths will lead to strong S*, at least at the lower frequencies. Figure 11 compares spherical point explosion synthetics with the tamped explosion accelerometer records at 710 m from the source. Not only the P, but the large S arrival at approximately 0.6 seconds is well matched by the synthetics without shear wave generation at the source.

Figure 12 shows an example that confirms the additional shear wave energy observed from the partially decoupled explosions vs the tamped explosion in the 30 to 50 Hz range. It shows the vertical component records at the same station, 145.4 and 163.2 m, respectively, from the tamped (solid) explosion and the partially decoupled (dashed) explosion at 26.5 m depth. The records are integrated to velocity from the accelerograms. The waveforms are very

similar, with a slight decrease in amplitude for the partially decoupled explosion up to 30 Hz. Above 30 Hz however, there is a large arrival only from the decoupled explosion, at approximately 0.2 seconds after P.

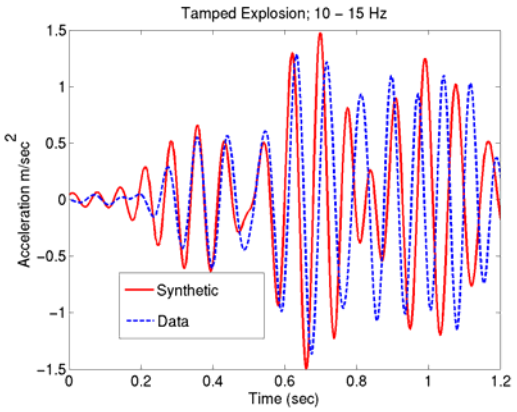

Figure 11. Spherical point explosion synthetics (red) and tamped explosion acceleration records (blue) at 710 m.

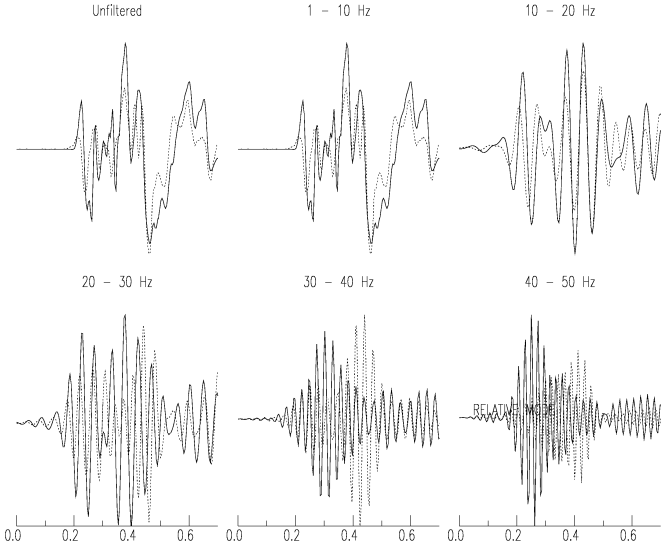

Figure 12. Vertical component records of the tamped (solid) explosion and the shallower partially decoupled explosion, at 145.4 and 163.2 m respectively. Initial P arrivals are aligned at 0.2 seconds.

CONCLUSIONS AND RECOMMENDATIONS

We find that an explosion offset from the center of a spherical cavity generates significant S waves and can be modeled as a dipole source. Numerical simulations predict reverberations with a distinct orientation in cavity decoupled explosions. The long duration coda of the Sterling decoupled explosion near field records can be explained by these numerical and analytical results. We further analyze and model local records from the Azgir tamped and water-filled cavity explosions. We identify two distinct shear wave arrivals, neither of which has the prominent 9 Hz bubble pulse peak seen in the P-wave spectra, indicating the S-waves were not scattered from P. The coda waves do have the resonance peak, indicating that the lack of the peak in the S-waves is not likely due to attenuation. A spherical explosion source does not match the observed shear waves. Rather, a CLVD source of comparable moment is required. The S-arrival times from the decoupled explosions are better matched by placing the CLVD at the explosion depth. The tamped explosion shear waves arrive slightly earlier and are better matched by making the CLVD component shallower. Numerical simulations indicate that neither an offset source or fracturing is the likely source of shear waves from these explosions. Preliminary analysis of records from the Israeli decoupling experiment indicates that the shear waves are generated by conversion of P waves, with one exception. At 30 to 50 Hz, the partially decoupled explosions have relatively more S-to-P energy, indicating that there is an S source at those frequencies that is absent from the tamped explosion source.

REFERENCES

Fisk, M (2007). Corner frequency scaling of regional Seismic phases for underground nuclear explosions at the Nevada Test Site, *Bull. Seism. Soc. Am*. 97: 977–988.

Gitterman, Y., R. Hofstetter, and V. Pinsky (2007). Depth-of-burial and decoupling explosion experiments in Israel: near-source and near-regional seismic energy generation, in *Proceedings of the 29th Annual Monitoring Research Review: Ground-Based Nuclear Explosion Technologies,* LA-UR-07-5613, Vol. 1, pp. 571–581.

Langston, C. A. (1983). Kinematic analysis of strong motion P and SV waves from the Sterling event. *J. Geophys. Res.* 88: 3486–3497.

Stevens, Jeffry L., Heming Xu, and G. E. Baker (2007). Analysis of shear wave generation by decoupled and partially coupled explosions, in *Proceedings of the 29th Annual Monitoring Research Review: Ground-Based Nuclear Explosion Technologies,* LA-UR-07-5613, Vol. 1, pp. 664–673.